Acta Biomaterialia xxx (2017) xxx–xxx

Contents lists available at ScienceDirect

Acta Biomaterialia

journal homepage: www.elsevier.com/locate/actabiomat

Full length article

Targeted glioma chemotherapy by cyclic RGD peptide-functionalized reversibly core-crosslinked multifunctional poly(ethylene glycol)-*b*-poly(ε-caprolactone) micelles

Ya Fang, Yu Jiang, Yan Zou, Fenghua Meng *, Jian Zhang, Chao Deng, Huanli Sun, Zhiyuan Zhong *

Biomedical Polymers Laboratory, and Jiangsu Key Laboratory of Advanced Functional Polymer Design and Application, College of Chemistry, Chemical Engineering and Materials Science, Soochow University, Suzhou 215123, PR China

ARTICLE INFO

Article history:
Received 28 July 2016
Received in revised form 23 December 2016
Accepted 4 January 2017
Available online xxxx

Keywords:
Biodegradable micelles
Targeted delivery
Chemotherapy
Reduction-sensitive
Glioblastoma

ABSTRACT

Cyclic RGD peptide-functionalized reversibly core-crosslinked biodegradable poly(ethylene glycol)-*b*-poly(ε-caprolactone) (PEG-PCL) micelles (cRGD-RCCMs) were designed and developed for highly potent and targeted glioma chemotherapy. To achieve crosslinkable core, dithiolane-functionalized trimethylene carbonate (DTC) was incorporated into PCL block. Interestingly, cRGD-RCCMs displayed a high doxorubicin (DOX) loading content of ~18 wt%, small hydrodynamic size of ~50 nm, and excellent colloidal stability with minimum drug leakage under physiological conditions while fast DOX release under cytoplasmic-mimicking reductive environments. MTT, confocal microscopy and flow cytometry measurement results pointed out that cRGD-RCCMs with 30% cRGD surface density (cRGD30-RCCMs) showed an evident selectivity, efficient cytoplasmic drug release, and superior antitumor activity to clinically used pegylated liposomal doxorubicin (DOX-LPs) in $\alpha_v\beta_3$ integrin overexpressing U87MG glioblastoma cells. Strikingly, DOX-loaded cRGD30-RCCMs demonstrated a prolonged circulation time showing an elimination half-life of ~4.7 h, three times exceeding that of the non-crosslinked counterparts, and a remarkably enhanced tumor accumulation of 7.7%ID/g. Furthermore, *in vivo* therapeutic studies revealed that DOX-loaded cRGD30-RCCMs effectively suppressed tumor growth, significantly prolonged survival time, and lessened side effects in subcutaneous U87MG glioblastoma-bearing nude mice. These reversibly core-crosslinked multifunctional biodegradable micelles might be developed into advanced and clinically viable targeted anticancer nanomedicines.

Statement of Significance

Nanomedicines based on biodegradable micelles and nanoparticles offer a most promising treatment for malignant tumors. The therapeutic outcomes of current nanomedicines are, however, trimmed by their instability, low tumor retention, inefficient tumor cell uptake, and inferior drug release control. We report herein that cRGD-functionalized, rapidly glutathione-responsive, and reversibly core-crosslinked biodegradable micellar doxorubicin based on PEG-PCL block copolymer mediates potent and targeted glioma chemotherapy, affording significantly better treatment efficacy and lower systemic toxicity than the non-crosslinked micellar doxorubicin and clinically used pegylated liposomal doxorubicin controls. These reversibly core-crosslinked multifunctional biodegradable micelles have emerged as a robust, simple, versatile, and safe nanoplatform that might elegantly bridge the gap between the scientific and translational anticancer nanomedicine research.

1. Introduction

Cancer chemotherapy though widely used in the clinics is challenged by its lacking tumor cell selectivity and severe dose-limiting side effects. The last decade has witnessed the rapid advance of polymeric nanomedicines, especially biodegradable

* Corresponding authors.
E-mail addresses: fhmeng@suda.edu.cn (F. Meng), zyzhong@suda.edu.cn (Z. Zhong).

http://dx.doi.org/10.1016/j.actbio.2017.01.007
1742-7061/

polymeric micellar nanomedicines, owing to their advantageous features like improved drug water solubility and bioavailability, prolonged blood circulation time, passive targeting to tumor vasculature *via* enhanced permeability and retention (EPR) effect, and decreased side effects [1,2]. Notably, a range of biodegradable polymeric micellar anticancer nanomedicines *e.g.* based on polyesters and polypeptides that enjoy excellent biocompatibility and safety profile have been developed to clinical or preclinical assessments [3,4]. For instance, micellar paclitaxel (PTX) based on poly (ethylene glycol)-*b*-poly(D,L-lactide) (PEG-PLA), Genexol-PM, has become one of the very few nanomedicines approved for treating breast, lung and ovarian cancers [5–7]. Langer et al. developed prostate-specific membrane antigen (PSMA)-targeted micellar docetaxel (DTX), BIND-014, based on PEG-*b*-poly(lactide-*co*-glycolide) (PEG-PLGA), for the treatment of several advanced solid tumors [8]. The clinical results showed that these micellar anticancer drugs, however, have comparable or marginally improved treatment benefits with regards to clinically used formulations. The suboptimal therapeutic efficacy of micellar anticancer drugs is likely a result of lacking *in vivo* stability, low tumor accumulation, poor tumor cell uptake and inferior intracellular drug release [2,9].

To enhance their *in vivo* antitumor efficacy, various types of multifunctional biodegradable micelles have been designed and studied in different tumor models [10–15]. For example, to address the *in vivo* instability and poor intracellular drug release problems, we and others have devised disulfide-crosslinked biodegradable micelles, which showed better stability, enhanced cytoplasmic drug release, and increased blood circulation time as compared to their non-crosslinked counterparts, leading to improved antitumor effect *in vitro* and *in vivo* [16–19]. It is interesting to note that fast redox-responsive or pH-responsive drug release could effectively reverse the multidrug resistance that is a challenge for cancer treatment [20,21]. To increase their tumor selectivity and accumulation [22,23], biodegradable micelles have been functionalized with various tumor specific ligands like peptides (*e.g.* cRGD peptides), antibodies or antibody fragment, and small molecules (*e.g.* folic acid, galactose) [24–30]. Nevertheless, as targeted nanomedicines were primarily based on non-crosslinked nanocarriers, their targeting effect though improved was not optimal and accompanied with pronounced side effects, partly due to insufficient *in vivo* stability and premature drug release [31,32]. Clearly, "active tumor targeting" nanomedicines should be based on stable and robust systems [33,34].

It should further be noted that reported multifunctional nanomedicines are typically associated with complicated design, complex preparation, unclear safety or low drug loading, which hampers their clinical translation [35,36]. The lessons from the few FDA approved nanomedicines such as Doxil® (pegylated liposomal DOX) and Abraxane® (albumin-PTX) reveal that straightforward and simplicity in preparation are pivotal in translational medicines [3,37–39].

In this article, we designed and developed cRGD-functionalized reversibly core-crosslinked multifunctional biodegradable micelles based on poly(ethylene glycol)-*b*-poly(ε-caprolactone) (PEG-PCL) (cRGD-RCCMs) for highly potent and targeted glioma chemotherapy (Scheme 1). To achieve disulfide-crosslinkable core, a recently developed proprietary monomer, dithiolane-functionalized trimethylene carbonate (DTC) that contains a pendant pseudo lipoic ring [40], was incorporated into PCL block. We have shown that lipoic acid functionalized polymeric micelles and nanoparticles can be readily crosslinked by forming linear polydisulfides *via* ring-opening polymerization while rapidly decrosslinked inside the tumor cells [18,20]. With DTC monomer, we have prepared crosslinked micellar nanoparticles based on cRGD-PEG-PDTC that have a size of ca. 182 nm after loading 14.4 wt% DOX [40] and crosslinked polymersomes based on cNGQ-PEG-P(TMC-DTC) for efficient loading and delivery of DOX·HCl (hydrophilic) [41]. cRGD was reported to have high affinity to tumor neovasculature as well as certain malignant tumors like glioma and melanoma [42–44]. We found that cRGD-decorated shell-sheddable PEG-SS-PCL micelles, which trigger drug release by shedding off PEG shells, mediate enhanced DOX delivery to U87MG glioma *in vivo* [45]. To the best of our knowledge, this represents the first report on active tumor-targeting, redox-sensitive and core-crosslinked biodegradable PEG-PCL micellar nanomedicines that are robust, multifunctional and simple to prepare. The clinical translation of nanomedicines is challenged by lack of straightforward and multifunctional nanoplatforms.

2. Materials and methods

2.1. Synthesis of diblock copolymer PEG-P(CL-DTC) and cRGD-PEG-P(CL-DTC)

cRGD-PEG-P(CL-DTC) was synthesized through three steps. A macroinitiator α-squaric acid ethylester–ω-hydroxyl-poly(ethylene glycol) (SAE-PEG-OH) was synthesized by dropwise adding 15 mL of aqueous solution of HO-PEG-NH_2 (M_n = 7.5 kg/mol, 1.125 g, 0.15 mmol) and triethylamine (75 mg, 0.75 mmol) into an ethanol solution (15 mL) of diethyl squarate (127.5 mg, 0.75 mmol) at 0 °C followed by stirring at 25 °C for 16 h. SAE-PEG-OH was purified by extensive dialysis in ethanol for 3 h (2 times change of media) and in water for 20 h (6 times change of media), and recovered by lyophilization. Yield: 80%. ^{1}H NMR (600 MHz, DMSO-d_6): PEG: δ 3.51, 4.55, 8.78, and 8.61; SAE moieties: δ 4.65 and 1.36. SAE functionality was determined to close to 100%.

Secondly, SAE-PEG-P(CL-DTC) was synthesized *via* ring-opening copolymerization of CL and DTC in anhydrous DCM at 40 °C using zinc bis[bis(trimethylsilyl)amide] and SAE-PEG-OH as an initiating system. Typically, in a nitrogen glove box, into a stirred solution of SAE-PEG-OH (150 mg, 20 μmol), CL (80 mg, 0.702 mmol) and DTC (40 mg, 0.208 mmol) in DCM (5.0 mL) was quickly added zinc bis [bis(trimethylsilyl)amide] (4 mg, 10 μmol) in DCM (0.2 mL). The polymerization proceeded under stirring at 40 °C for 24 h. The polymers were recovered by twice precipitation from cold diethyl ether. Yield: 88%. ^{1}H NMR (600 MHz, DMSO-d_6): PEG: δ 3.51, 8.78, and 8.61; DTC: δ 3.06, and 4.16–4.27; CL: δ 1.30, 1.54, 2.27–2.35, and 3.98–4.07. SAE moieties: δ 4.65 and 1.36. M_n (^{1}H NMR) = 13.2 kg/mol, M_n (GPC) = 35.9 kg/mol, Đ = 1.32.

Finally, cRGD-PEG-P(CL-DTC) was obtained by adding 1.5 mL of DMSO solution of SAE-PEG-P(CL-DTC) (120 mg, 11 μmol) into 4.5 mL of borate buffer (0.01 M, pH 9.1) containing cRGD*f*K (13.6 mg, 22 μmol), and stirring at r.t. for 16 h, followed by extensive dialysis (MWCO 3500 Da) for 48 h in deionized water. Yield: 92%. ^{1}H NMR (600 MHz, DMSO-d_6): cRGD moiety: δ 7.22. BCA protein and TNBSA assays showed a cRGD functionality of 100% and 98.4%, respectively.

The synthesis of PEG-P(CL-DTC) was the same as for SAE-PEG-P(CL-DTC) except that MeO-PEG-OH (M_n = 5.0 kg/mol) was used as a macroinitiator. Yield: 89%. ^{1}H NMR (400 MHz, $CDCl_3$): PEG: δ 3.38, 3.65; DTC: δ 3.06, 4.23–4.33; CL: δ 1.38, 1.65, 2.30–2.38, and 4.05–4.15. M_n (^{1}H NMR) = 10.7 kg/mol. M_n (GPC) = 28.5 kg/mol, Đ (GPC) = 1.49.

2.2. Preparation of cRGD-RCCMs and DOX-cRGD-RCCMs

In brief, 200 μL of DMF solution (5 mg/mL) of cRGD-PEG-P(CL-DTC) and PEG-P(CL-DTC) at a predetermined weight ratio was injected into 800 μL of phosphate buffer (PB, 10 mM, pH 7.4) and

Please cite this article in press as: Y. Fang et al., Targeted glioma chemotherapy by cyclic RGD peptide-functionalized reversibly core-crosslinked multifunctional poly(ethylene glycol)-*b*-poly(ε-caprolactone) micelles, Acta Biomater. (2017), http://dx.doi.org/10.1016/j.actbio.2017.01.007

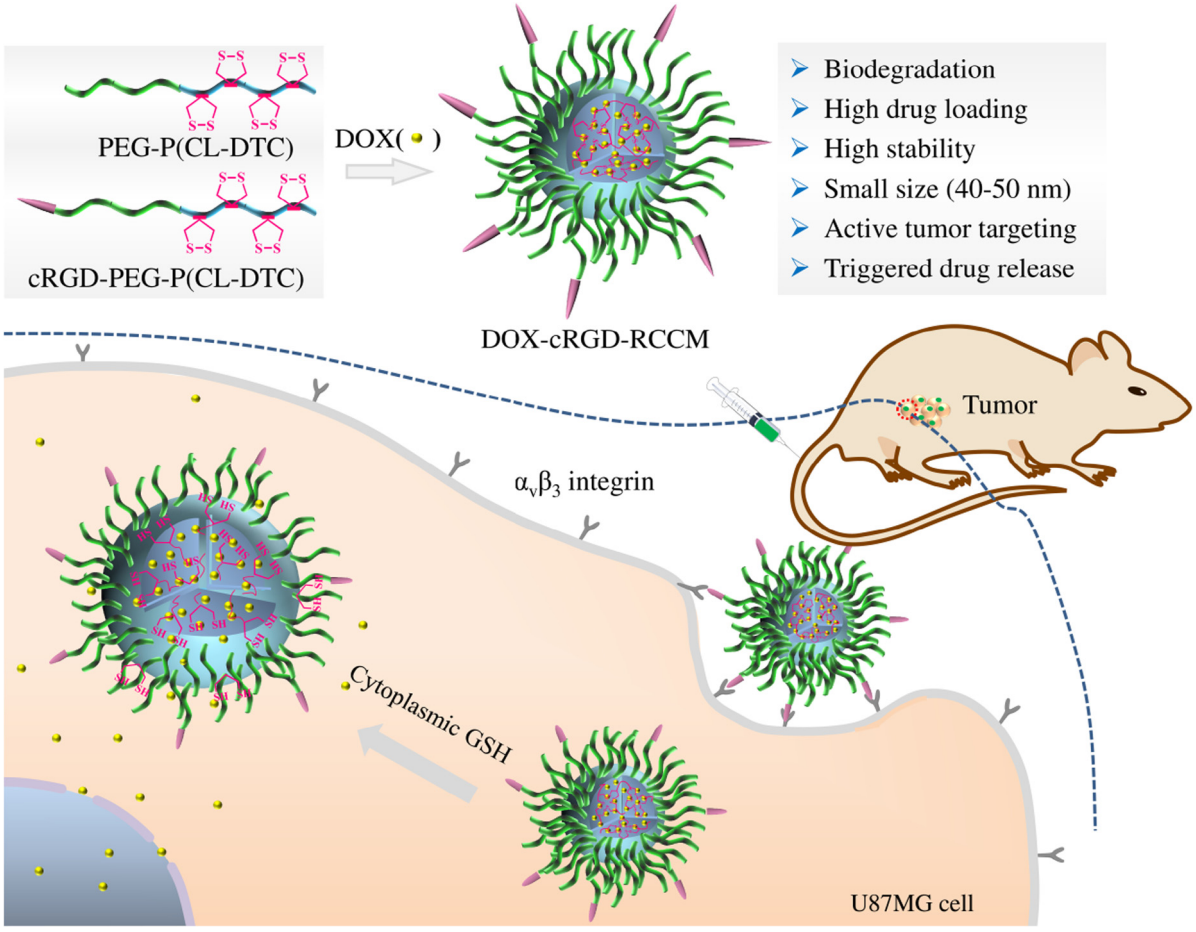

Scheme 1. cRGD-functionalized and reversibly core-crosslinked multifunctional PEG-PCL micelles (cRGD-RCCMs) for highly potent and targeted glioma chemotherapy.

stood at 37 °C for 2 h. The obtained micellar dispersion was dialyzed against PB (MWCO 3500 Da) at r.t. for 24 h. The micelles were self-crosslinked during the dialysis procedure. The obtained micelles were named as cRGDX-RCCMs, where X stands for weight percentage of cRGD-PEG-P(CL-DTC) in the polymer mixture. DOX-loaded micelles (DOX-cRGD-RCCMs) were prepared similarly except that the copolymer solution containing certain amount of desalted DOX was used.

2.3. MTT assays

MTT assays were performed in $\alpha_v\beta_3$ over-expressing U87MG cells in DMEM media. To investigate the antitumor efficacy and targetability of DOX-cRGD-RCCMs, 10 μL of micelles with cRGD contents from 0 to 30% and DOX dosages from 0.01 to 40 μg/mL in PBS were tested. The cells were treated with DOX-cRGD-RCCMs for 4 h, the media were removed and replaced by fresh media, and the cells were further cultured for 68 h. 10 μL of PBS solution of MTT (5 mg/mL) was added. After 4 h, the MTT-formazan generated by live cells was dissolved in 150 μL of DMSO. The absorbance (492 nm) was measured using a microplate reader as reported previously [40]. The cell viability (%) was determined by comparing the absorbance at 492 nm with control wells containing only cells (100%). Data were given as average ± SD (n = 4). Commercial pegylated liposomal doxorubicin (DOX-LPs) was used as a control. The cytotoxicity of empty cRGD-RCCMs was assessed using U87MG cells following 72 h incubation at a concentration of 0.5 or 1.0 mg/mL.

2.4. Flow cytometric analysis and confocal microscopy measurements

For flow cytometric measurements, U87MG cells were seeded in a 6-well plate (1×10^6 cells/well) containing 900 μL of DMEM medium. After 48 h, 100 μL of DOX-cRGD30-RCCMs, DOX-RCCMs or DOX-LPs in PBS (20 μg DOX/mL) was added. After 4 h incubation at 37 °C, the cells were digested by 0.25% (w/v) trypsin and 0.03% (w/v) EDTA. The suspensions were handled and measured using a flow cytometer (Beckton Dickinson, USA) as reported previously [40]. The inhibitive experiments were conducted by the pre-treatment of U87MG cells with free cRGD solution (2 mg/mL) for 2 h before incubation with DOX-cRGD-RCCMs.

In CLSM studies, U87MG cells on microscope slides in 24-well plates (1×10^5 cells/well) were incubated with DOX-cRGD30-RCCMs, DOX-RCCMs or DOX-LPs (10 μg DOX/mL) at 37 °C for 4 h. The cells were further cultured in fresh medium for 4 or 8 h, washed with PBS (×3), fixed with 4% paraformaldehyde solution (20 min) and washed with PBS (×3). 4,6-Diamidino-2-phenylindole (DAPI) was used to stain cell nuclei before observation using CLSM (TCS SP5).

2.5. Animal models

All animal procedures were handled under protocols approved by Soochow University Laboratory Animal Center and the Animal Care and Use Committee of Soochow University. Nude mice (18–22 g, 5 weeks, Model Animal Research Center of Nanjing University) were inoculated subcutaneously on the hind flank with U87MG human glioblastoma cells (1×10^7 per mouse in 50 μL).

Please cite this article in press as: Y. Fang et al., Targeted glioma chemotherapy by cyclic RGD peptide-functionalized reversibly core-crosslinked multifunctional poly(ethylene glycol)-*b*-poly(ε-caprolactone) micelles, Acta Biomater. (2017), http://dx.doi.org/10.1016/j.actbio.2017.01.007

When the tumor size reached ca. 100–150 mm^3, U87MG active mass was taken and cut into small cubes of ca. 2 mm^3, and quickly inoculated subcutaneously into the right flank of the nude mice. Mice with tumor size of ca. 150 ~ 200 mm^3 were used for *in vivo* imaging and biodistribution studies, and mice with tumor size of ca. 30 ~ 50 mm^3 for therapeutic studies.

2.6. In vivo pharmacokinetics and fluorescence imaging

To determine the blood circulation, Kunming mice were intravenously injected *via* tail vein (n = 3) with 200 μL of DOX-cRGD30-RCCMs, DOX-RCCMs, DOX-LPs, or free DOX·HCl (10 mg DOX equiv./kg). At predetermined time points after *iv* injection, ca. 10 μL of blood was taken from retro-orbital sinus of mice. The samples upon withdrawing were immediately added in 0.1 mL of Triton X-100 solution (1%) with brief sonification. DOX was extracted by incubating blood samples in 900 μL of extraction solution (DMF solution containing 20 mM DTT) at −4 °C for 10 h. After centrifugation at 20 krpm for 20 min, DOX level in the supernatant was measured using fluorometry. In the pharmacokinetics curves, the half-lives of the distribution phase ($t_{1/2,\alpha}$) and elimination phase ($t_{1/2,\beta}$) were calculated by fitting the experimental data using Software Origin 8 exponential decay 2 model: $y = A_1 \times \exp(-x/t_1) + A_2 \times \exp(-x/t_2) + y_0$, and taking $t_{1/2,\alpha} = 0.693 \times t_1$ and $t_{1/2,\beta} = 0.693 \times t_2$. The area under the curve (AUC) was calculated by the following formulas: AUC (ng h/mL) = $A_1 \times t_1 + A_2 \times t_2$.

In order to visualize the drug distribution *in vivo*, a NIR probe DIR was used as a model. Mice bearing U87MG tumor xenograft were randomly grouped and injected with 200 μL of DIR-loaded cRGD-RCCMs or RCCMs (20 μg DIR/mL) *via* tail vein. At prescribed time points (2, 4, 6, 8, 12, 24 and 36 h) after *i.v.* injection, isoflurane was injected to each mice for anesthesia, and 3% isoflurane was continuously delivered *via* a nose cone system during the imaging acquiring process. The fluorescent images were taken using a Kodak near-infrared fluorescence imaging system at ex. 747 nm/em. 774 nm. All images were acquired and analyzed using Lumia II software. The mouse auto fluorescence was removed by spectral unmixing.

2.7. In vivo biodistribution and therapeutic efficacy

For *in vivo* biodistribution studies, nude mice bearing U87MG tumors were randomly grouped and intravenously injected with 200 μL of DOX-cRGD-RCCMs (10 mg DOX equiv./kg) *via* tail vein. The mice were sacrificed at 4, 8 or 24 h post injection. The major organs as well as tumors were collected, washed with saline, dried with towel, weighed, and homogenized in lysis solution (DMF containing 20 mM DTT) to extract DOX. After 24 h incubation, the samples were centrifuged at 15 krpm for 20 min, and DOX level in supernatant was determined by fluorometry (n = 3).

For evaluation of antitumor efficacy, nude mice bearing U87 tumors were weighed and randomly divided into 6 groups (n = 6). 200 μL of DOX-cRGD-RCCMs, DOX-RCCMs or DOX-LPs (10 mg DOX equiv./kg) were injected *via* tail vein on day 0, 3, 6, 9, and 12. PBS was used as a control. Every two days the tumor size was measured using digital calipers, and tumor volume was calculated according to the formula $V = 0.5 \times L \times W \times H$, wherein L, W and H are the tumor length, width and height, respectively. The relative tumor volume was defined as V/V_0 (V_0 is the tumor volume on day 0). Every two days the body weights of the mice were measured and normalized to their initial weights. On day 20, the treatment was terminated, from each group one mouse was taken and sacrificed by cervical vertebra dislocation. The liver, heart, kidney and tumors were taken for histological analysis using hematoxylin and eosin (H&E) staining followed by microscopic observation (Olympus BX 41 microscope) [40]. The rest five mice were used to observe the Kaplan–Meier survival curves within 66 days. Mice were considered dead either when the mice died during treatment or when the tumor volume reached 1000 mm^3.

2.8. Statistical analysis

Data were presented as average ± s.d. Differences between two groups were assessed using the paired, two-sided Student *t*-test. $^{*}p < 0.05$ was considered significant, and $^{**}p < 0.01$ and $^{***}p < 0.001$ were considered highly significant.

3. Results and discussion

3.1. Synthesis of PEG-P(CL-DTC) and cRGD-PEG-P(CL-DTC) block copolymers

With an aim of developing cRGD-functionalized reversibly core-crosslinked multifunctional poly(ethylene glycol)-*b*-poly(ε-caprolactone) (PEG-PCL) micelles (cRGD-RCCMs) for targeted glioma chemotherapy (Scheme 1), we devised and synthesized two dithiolane-functionalized PEG-PCL diblock copolymers, PEG-P(CL-DTC) and cRGD-PEG-P(CL-DTC), by ring opening polymerization (ROP) of ε-caprolactone (CL) with dithiolane-functionalized trimethylene carbonate (DTC). PEG-P(CL-DTC) was obtained using CH_3O-PEG-OH (M_n = 5.0 kg/mol) as an initiator at a CL/DTC/PEG molar ratio of 35/10/1 (Scheme 2A). ^{1}H NMR displayed besides signals attributable to PEG (δ 3.65, 3.38) also resonances assignable to DTC moieties (δ 3.06, 4.23–4.33) and CL moieties (δ 1.38, 1.65, 2.30–2.38, 4.05–4.14) (Fig. 1). Notably, signals at δ 4.23 assignable to the methylene protons of DTC units directly linking to CL (–OC(O)OCH_2C($C_2H_4S_2$)CH_2OC(O)–CL–) and signals at δ 4.15 and 2.38 attributable to the two methylene protons of CL units next to DTC (–$CH_2CH_2CH_2CH_2CH_2$OC(O)O–DTC– and –DTC–OC(O)CH_2CH_2-$CH_2CH_2CH_2$O–) were detected, supporting statistical copolymerization of DTC and CL. The degree of polymerization (DP) of DTC and CL could be determined by comparing the integrals of dithiolane signals of DTC moieties at δ 3.06 and the methylene protons of CL moieties at δ 2.30–2.38 to the methylene protons of PEG at δ 3.65, respectively. The results showed that PEG-P(CL-DTC) had a controlled M_n of 5.0–(3.9–1.9) kg/mol, which was close to the design (Table 1). Gel permeation chromatography (GPC) measurements displayed a unimodal distribution with a moderate M_w/M_n of 1.49. DSC analyses showed a single melting temperature (T_m) of ca. 54.7 °C due to PEG block and a glass transition temperature (T_g) of ca. −18 °C, indicating that P(CL-DTC) block is amorphous and in a rubbery state at r.t., confirming that DTC and CL form a statistical copolymer and P(CL-DTC) block is compatible with PEG.cRGD-PEG-P(CL-DTC) was synthesized *via* ROP of CL and DTC using squaric acid ethylester end-functionalized PEG (SAE-PEG-OH, M_n = 7.5 kg/mol) as a macro-initiator followed by coupling with cRGD*f*K (cRGD) (Scheme 2B). Squaric acid diethyl ester (SADE) has a high reactivity toward amidation [46,47]. The treatment of NH_2-PEG-OH (M_n = 7.5 kg/mol) with SADE at neutral pH afforded SAE-PEG-OH. Interestingly, SADE once forming an amide, the other ester has a reduced reactivity at neutral pH [48], circumventing coupling of two PEG to one SADE. ^{1}H NMR showed peaks at δ 4.65 and 1.36 assignable to methylene and methyl proton of SAE moieties, and the signals at δ 8.61–8.77 to the amide protons (Fig. S1A). By comparing the signal integrals at δ 1.36 with δ 3.63 (PEG methylene protons), a quantitative functionality of SAE-PEG-OH with SAE was concluded. MALDI-TOF spectrum further confirmed the complete conversion of NH_2-PEG-OH to SAE-PEG-OH (Fig. S2). The copolymerization of DTC and CL using SAE-PEG-OH as a macro-initiator yielded SAE-PEG-P(CL-DTC) with an M_n of 7.5–(3.8–1.9) kg/mol, as determined by ^{1}H NMR and a moderate

Please cite this article in press as: Y. Fang et al., Targeted glioma chemotherapy by cyclic RGD peptide-functionalized reversibly core-crosslinked multifunctional poly(ethylene glycol)-*b*-poly(ε-caprolactone) micelles, Acta Biomater. (2017), http://dx.doi.org/10.1016/j.actbio.2017.01.007

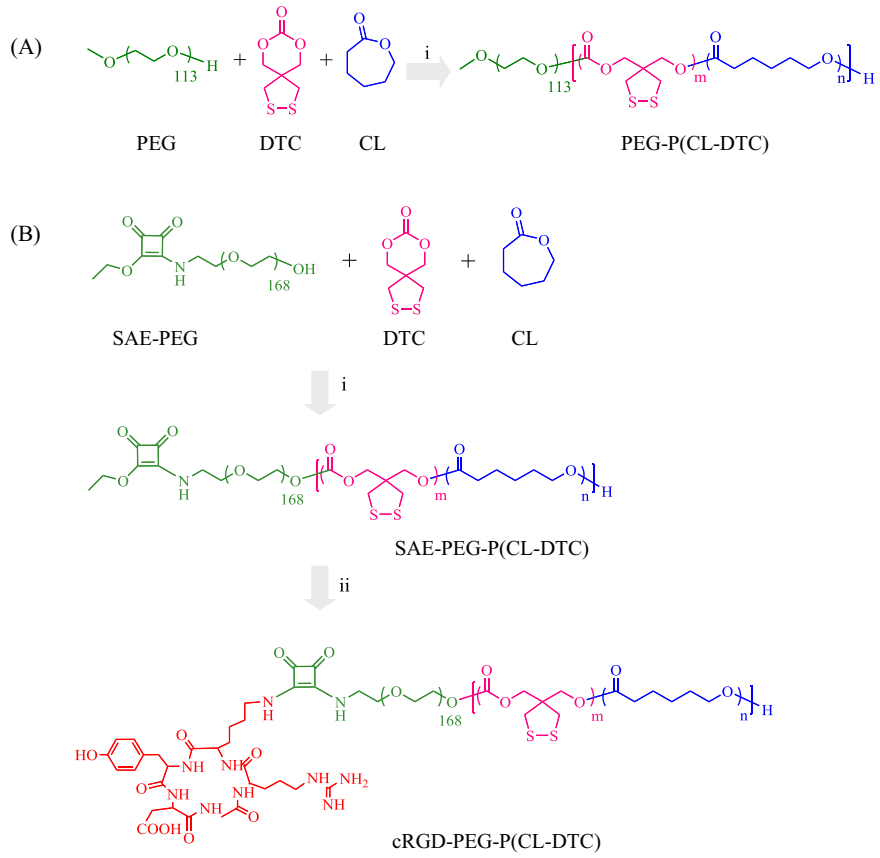

Scheme 2. Synthesis of PEG-P(CL-DTC) (A) and cRGD-PEG-P(CL-DTC) (B). Conditions: (i) zinc bis[bis(trimethylsilyl) amide], CH_2Cl_2, 40 °C, 24 h; (ii) cRGD*f*K, borate buffer (pH 9.1)/DMSO (3/1, v/v), 25 °C, 20 h.

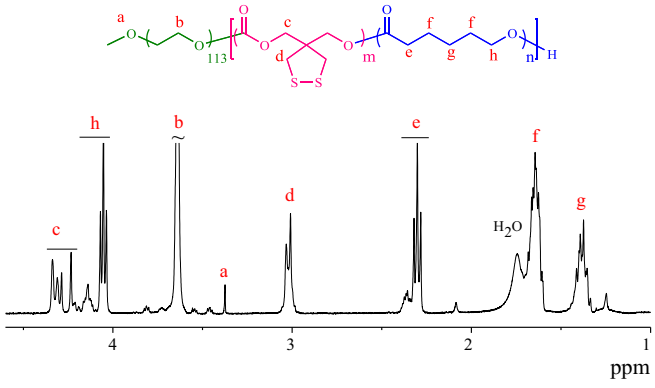

Fig. 1. ^{1}H NMR spectrum (400 MHz, $CDCl_3$) of PEG-P(CL-DTC).

M_w/M_n of 1.32, as shown by GPC (Table 1). Importantly, SAE groups remained intact during ROP (Fig. S1B). The treatment of SAE-PEG-P(CL-DTC) with cRGD*f*K at pH 9 gave cRGD-PEG-P(CL-DTC). ^{1}H NMR spectrum displayed that the peak at δ 4.65 assignable to SAE methylene proton disappeared and the characteristic peaks of cRGD appeared at δ 7.22 (Fig. S1C). Both BCA and TNBSA assays revealed a cRGD functionality of over 98 %.

3.2. Preparation and characterization of DOX-loaded cRGD-RCCMs (DOX-cRGD-RCCMs)

cRGD-functionalized reversibly core-crosslinked PEG-PCL micelles (cRGD-RCCMs) were readily prepared by solvent exchange method from PEG-P(CL-DTC) and cRGD-PEG-P(CL-DTC) copolymers. Fig. 2A shows that RCCMs and cRGD-RCCMs with cRGD densities ranging from 10% to 30% had small hydrodynamic sizes of 40–50 nm and low polydispersity index (PDI) of 0.10. TEM micrograph confirmed their spherical morphology and small particle size. Notably, no critical micelle concentration (CMC) was detected for all micelles following work-up, indicating that micelles were crosslinked (Fig. S3). UV measurements revealed complete disappearance of absorbance at 320 nm characteristic

Table 1
Synthesis of PEG-P(CL-DTC) and SAE-PEG-P(CL-DTC) block copolymers.

Entry	Copolymer	M_n (kg/mol)		M_w/M_n[b]	T_g[c] (°C)
		Design	Determined[a]		
1	PEG-P(CL-DTC)	5.0–(4.0–2.0)	5.0–(3.9–1.9)	1.49	−18.2
2	SAE-PEG-P(CL-DTC)	7.5–(4.0–2.0)	7.5–(3.8–1.9)	1.32	−17.4

[a] Determined by ^{1}H NMR.
[b] Determined by GPC.
[c] Determined by DSC.

Please cite this article in press as: Y. Fang et al., Targeted glioma chemotherapy by cyclic RGD peptide-functionalized reversibly core-crosslinked multi-functional poly(ethylene glycol)-*b*-poly(ε-caprolactone) micelles, Acta Biomater. (2017), http://dx.doi.org/10.1016/j.actbio.2017.01.007

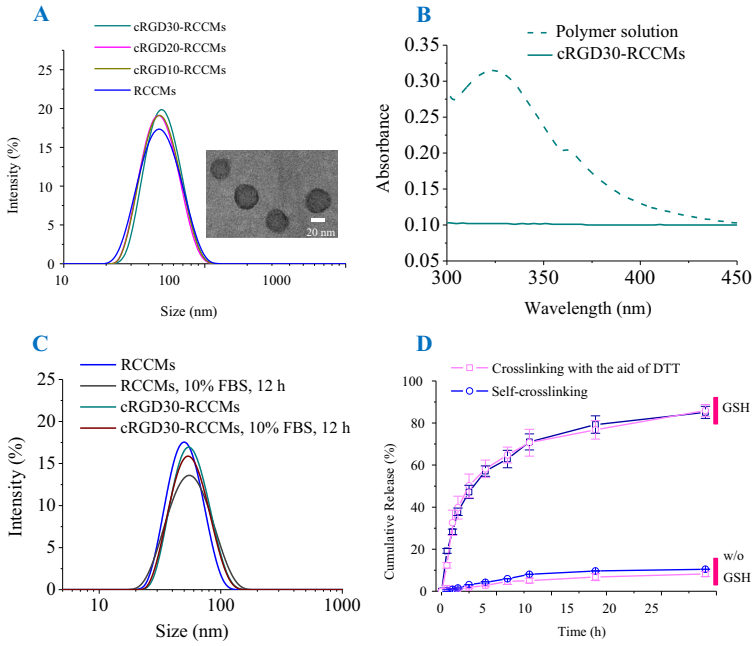

Fig. 2. Characterizations of RCCMs and cRGD-RCCMs. (A) Size distribution profiles determined by DLS at a micellar concentration of 1 mg/mL (Inset: TEM image). (B) UV spectra of cRGD30-RCCMs in PB and the corresponding polymer solution in DMF (micellar concentration: 10 mg/mL). (C) Stability of micelles in cell culture medium containing 10% FBS (micellar concentration: 1 mg/mL). (D) The *in vitro* DOX release at 37 °C from DOX-RCCMs obtained by either auto-crosslinking or DTT-catalyzed crosslinking (micellar concentration: 30 μg/mL).

of dithiolane rings after work-up procedure (Fig. 2B), supporting that self-crosslinking takes place *via* the ring-opening polymerization of dithiolane in the micellar core, as also observed for PEG-PDTC micelles [40]. In accordance, both RCCMs and cRGD30-RCCMs were stable in culture medium containing 10% FBS (Fig. 2C). RCCMs and cRGD30-RCCMs showed a high drug loading efficiency toward DOX reaching a drug loading content of ~18 wt %. Importantly, DOX-cRGD-RCCMs maintained a small size (~50 nm) and a low PDI (Table 2). The high DOX loading was likely due to their high stability and reduced drug diffusion upon core-crosslinking. Notably, the *in vitro* drug release profiles demonstrated that DOX release from DOX-cRGD-RCCMs was minor (<10%) in 24 h under physiological conditions (pH 7.4, 37 °C), whereas 85% DOX was released with 10 mM glutathione (GSH) under otherwise the same conditions (Fig. 2D). DOX-cRGD-RCCMs crosslinked with aid of DTT also showed the same drug release behavior, corroborating a high-efficiency self-crosslinking. In comparison, PEG-PCL micelles were reported to have a relatively low DOX loading content (<11%) and a high drug leakage of ca. 30–40% in 24 h under physiological conditions [49,50]. DOX-cRGD-RCCMs with excellent stability, minimum drug leakage and fast redox-responsive drug release are superior to PEG-PCL micelles.

3.3. *In vitro* tumor cell selectivity and antitumor activity of DOX-cRGD-RCCMs

The cytotoxicity of blank and DOX-cRGD-RCCMs was estimated using MTT assays on $\alpha_v\beta_3$ integrin overexpressing U87MG glioblastoma cells. The results revealed that all empty RCCMs and cRGD-RCCMs (cRGD densities: 10%, 20% and 30%) were nontoxic at tested concentrations of 0.5 and 1.0 mg/mL (Fig. 3A). In contrast, DOX-RCCMs and DOX-cRGD-RCCMs showed high antitumor efficacy, and the half-maximal inhibitory concentration (IC_{50}) decreased from 10.8 to 1.9 μg/mL with increasing cRGD densities from 0 to 30% (Fig. 3B). Notably, DOX-cRGD30-RCCMs exhibited about 2.5-fold higher antitumor activity than the clinically used pegylated liposomal doxorubicin (DOX-LPs). These results imply that cRGD30-RCCMs can actively target to U87MG cells and liberate DOX to the cytoplasm. On the contrary, the non-targeting and non-crosslinked PEG-PCL micelles exhibited typically reduced *in vitro* antitumor activity due to inhibited intracellular drug release [50,51].

Flow cytometric analyses revealed that U87MG cells at 4 h incubation with DOX-RCCMs had ca. 3 times higher DOX intensity than those with DOX-LPs (Fig. 3C). Moreover, DOX-cRGD30-RCCMs

Table 2
Characterization of DOX-RCCMs and DOX-cRGD30-RCCMs.

Micelles	DOX feed ratio (wt%)	Size[a] (nm)	PDI [a]	DLC (wt%)[b]	DLE (%)[b]
RCCMs	10	46.6	0.10	7.9	85.5
	20	48.5	0.13	14.1	81.7
	30	52.2	0.11	18.7	76.5
cRGD30-RCCMs	10	49.5	0.13	7.5	81.5
	20	52.8	0.09	13.4	77.4
	30	55.3	0.18	17.9	72.7

[a] Determined in phosphate buffer (PB, 1 mg/mL) by DLS at 25 °C.
[b] Determined by fluorescence measurement.

Please cite this article in press as: Y. Fang et al., Targeted glioma chemotherapy by cyclic RGD peptide-functionalized reversibly core-crosslinked multifunctional poly(ethylene glycol)-*b*-poly(ε-caprolactone) micelles, Acta Biomater. (2017), http://dx.doi.org/10.1016/j.actbio.2017.01.007

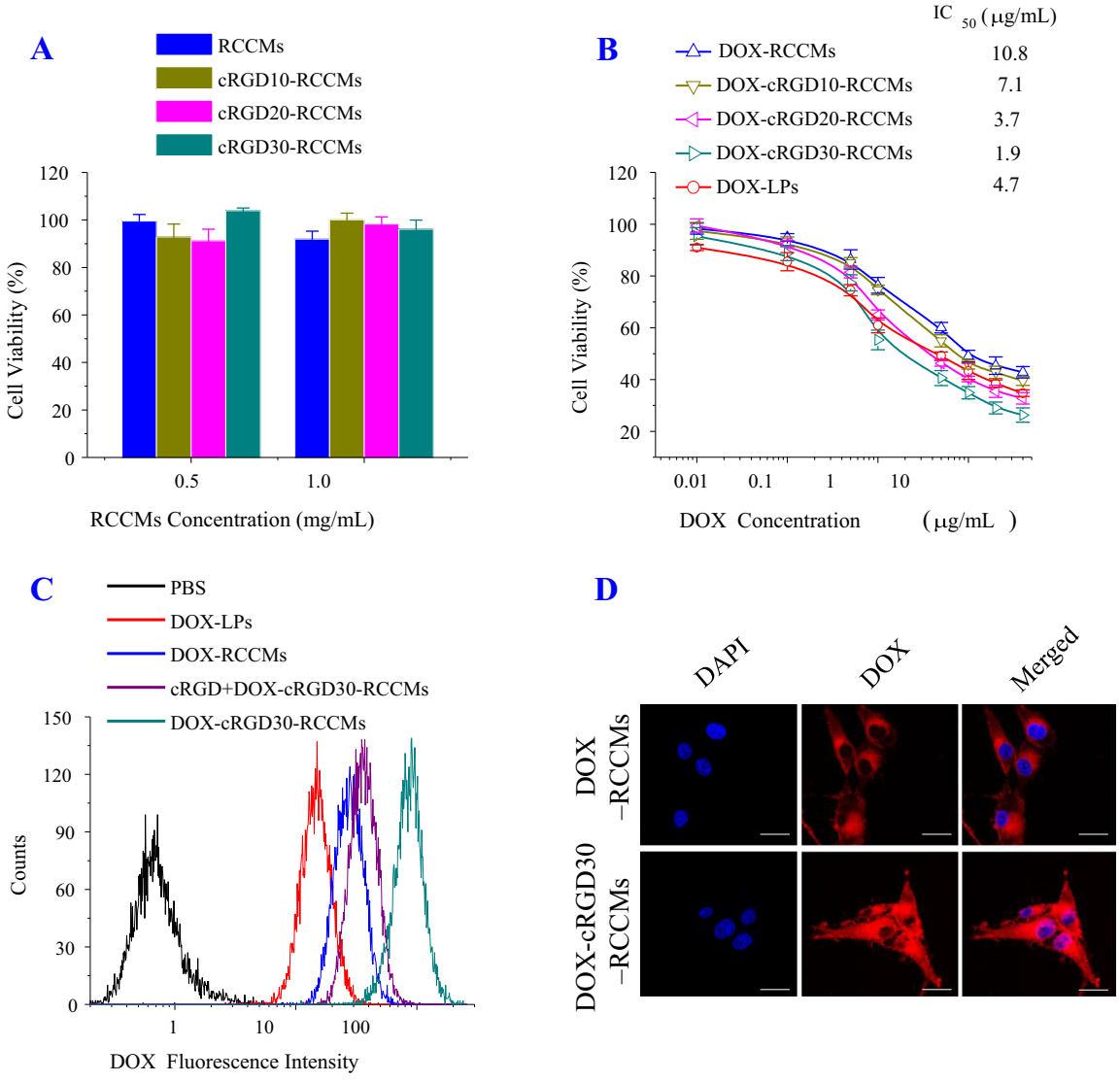

Fig. 3. *In vitro* cell experiments using U87MG cells. (A) MTT assays of bare cRGD-RCCMs and RCCMs following 72 h incubation (n = 4). (B) The antitumor activity of DOX-cRGD-RCCMs. The cells were incubated for 4 h and further cultured in fresh media for 68 h. (C) Flow cytometric analysis of U87MG cells following 4 h incubation with DOX-cRGD30-RCCMs, DOX-RCCMs or DOX-LPs (10.0 μg DOX/mL). The inhibitive experiment was conducted by pretreating U87MG cells with cRGD (2 mg/mL) before adding DOX-cRGD30-RCCMs. (D) CLSM images of U87MG cells following 12 h incubation with DOX-cRGD30-RCCMs or DOX-RCCMs (10.0 μg DOX /mL). The scale bar corresponds to 20 μm.

displayed further 3 times improvement in DOX uptake as compared to DOX-RCCMs, in line with active targeting effect of cRGD30-RCCMs. The inhibition experiment demonstrated that 2 h pretreatment of U87MG cells with cRGD (2 mg/mL) before the addition of DOX-cRGD30-RCCMs resulted in a marked decrease of cellular uptake (Fig. 3C). CLSM images showed that U87MG cells following 12 h incubation with DOX-cRGD30-RCCMs gave strong fluorescence throughout whole cells, which was considerably higher than those with non-targeting DOX-RCCMs (Fig. 3D). DOX-LPs, however, only showed negligible DOX inside cells (data not shown). These results confirm that DOX-cRGD-RCCMs are endocytosed by U87MG cells *via* a receptor mediated mechanism, and DOX is quickly dumped into the cancer cells, bringing about high tumor cell selectivity and antitumor potency. It has been reported that cRGD-functionalized nanoparticles significantly increased their cellular uptake by U87MG cells *in vitro* and *in vivo* [42,52]. The *in vitro* cell selectivity and uptake of cRGD-functionalized nanoparticles depend intimately on their cRGD surface density, which varies from cells to cells [43,44].

3.4. In vivo pharmacokinetics and biodistribution studies

The *in vivo* pharmacokinetics of DOX-cRGD-RCCMs and DOX-RCCMs was investigated in Kunming mice following *i.v.* injection (10 mg DOX equiv./kg). The profiles of blood circulation followed a two-compartment model: a rapid declined distribution phase and a prolonged elimination phase (Fig. 4). Noteworthy, DOX-cRGD30-RCCMs exhibited an elimination half-life ($t_{1/2,\beta}$) of 4.7 h, which was, though shorter than DOX-LPs (8.3 h), 11.7- and 3.9-fold longer than those of free DOX ($t_{1/2,\beta}$ = 0.4 h) and non-crosslinked control DOX-cRGD30-PEG-PCL ($t_{1/2,\beta}$ = 1.2 h), underlying the significant role of crosslinking on the *in vivo* pharmacokinetics of micellar nanomedicines [21,34]. The quick elimination and low tumor retention was observed for many non-crosslinked micellar systems [53], as micelles tend to dissociate as result of large dilution, high shear force and interactions with plasma proteins [34]. DOX-cRGD30-RCCMs revealed 2.6- and 8.5-fold higher AUC than DOX-cRGD30-PEG-PCL and free DOX, respectively (Fig. 4, inset). The prolonged circulation of DOX-cRGD30-RCCMs

Please cite this article in press as: Y. Fang et al., Targeted glioma chemotherapy by cyclic RGD peptide-functionalized reversibly core-crosslinked multifunctional poly(ethylene glycol)-*b*-poly(ε-caprolactone) micelles, Acta Biomater. (2017), http://dx.doi.org/10.1016/j.actbio.2017.01.007

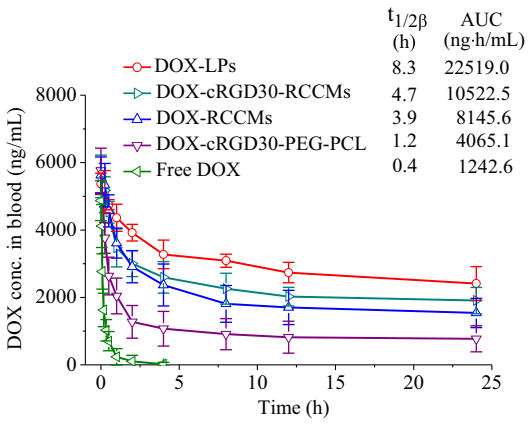

Fig. 4. The *in vivo* pharmacokinetics of DOX-cRGD30-RCCMs, non-targeting DOX-RCCMs, non-crosslinked DOX-cRGD30-PEG-PCL, DOX-LPs and free DOX in Kunming mice.

is likely a result of their high *in vivo* stability and small particle size.

To study the *in vivo* biodistribution, we loaded cRGD-RCCMs and RCCMs with a model hydrophobic near-infrared agent DIR and monitored DIR fluorescence in nude mice bearing U87MG tumors using an *in vivo* fluorescence imaging system after *i.v.* injection. The images displayed an obvious increase in tumor accumulation with time until 36 h for both micelles, with DIR-cRGD30-RCCMs having much higher DIR accumulation in the tumor than DIR-RCCMs (Fig. 5A), verifying the prominent tumor accumulation and retention. We further quantified DOX distribution in the tumors and major organs of U87MG-bearing nude mice at 8 h post *i.v.* injection. Remarkably, DOX-cRGD-RCCMs treated mice exhibited a tumor DOX level of 7.7%ID/g (injected dose per gram of tissue), significantly higher than those with DOX-RCCMs and DOX-LPs (Fig. 5B). Tumor/normal tissue distribution ratios (T/N) further confirmed that DOX-cRGD-RCCMs resulted in significantly higher tumor accumulation and selectivity than DOX-RCCMs and DOX-LPs (Fig. S4). Notably, DOX-cRGD-RCCMs achieved comparable drug accumulation to cRGD-functionalized drug-crosslinked micelles [44], and higher accumulation than cRGD and DOX-conjugated unimolecular micelles [54] and cRGD-functionalized robust PEG-PCL/gold nanorod hybrid micellar nanoparticles [42]. On the contrary, tumor accumulation of non-crosslinked and non-targeted PEG-PCL micelles was reported to be less than 2% ID/g [55] and 2.5%ID/g [54], respectively. It is evident, therefore, that the small-sized, robust and tumor active targeting cRGD-RCCMs are capable of efficiently loading and delivering DOX into U87MG glioma *in vivo*.

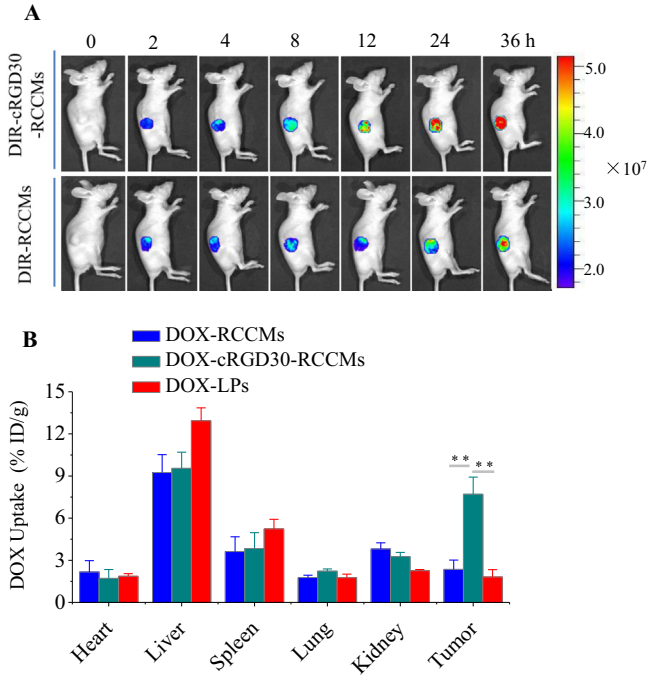

Fig. 5. (A) The *in vivo* fluorescence images of U87MG bearing nude mice at different time points following *i.v.* injection of 200 μL of DIR-loaded cRGD30-RCCMs or RCCMs (20 μg DIR/mL). (B) The *in vivo* DOX biodistribution in U87MG bearing nude mice at 8 h post injection of DOX-cRGD30-RCCMs, DOX-RCCMs or DOX-LPs (n = 3). Student's *t* test, $^{*}p < 0.05$, $^{**}p < 0.01$, and $^{***}p < 0.001$.

3.5. In vivo targeted chemotherapy of U87MG glioma-bearing nude mice

cRGD density is one of the most important parameters for micellar drugs in targeted chemotherapy. However, seldom is reported on its influence *in vivo*. Here, we studied the anti-glioblastoma effect of DOX-cRGD-RCCMs containing different cRGD contents using U87MG-bearing nude mice. Interestingly, it was demonstrated that all DOX-cRGD-RCCMs could retard tumor growth and the tumor inhibitive potency was obviously enhanced by increasing cRGD content (Fig. 6A). DOX-cRGD30-RCCMs showed significantly better tumor suppression than micelles with lower or no cRGD, while comparable to DOX-LPs. Here, free DOX was not used as a control since our previous studies have shown serious side effects in mice [20,42]. The photograph of tumor blocks excised on day 20 post injection confirmed the most effective tumor inhibition of DOX-cRGD30-RCCMs (Fig. 6B).

Notably, unlike DOX-LPs that led to serious side effects including drastic body weight loss and hand-foot syndrome, all DOX-cRGD-RCCMs formulations did not cause any obvious change in body weight and mouse behavior (Fig. 6C), indicating reduced systemic toxicity of DOX-cRGD-RCCMs as compared to DOX-LPs. Fig. 6D displays clearly that DOX-cRGD30-RCCMs markedly increased survival time of mice. The mice treated with DOX-cRGD30-RCCMs, non-targeting DOX-RCCMs, DOX-LPs and PBS had median survival times of 60, 36, 18 and 26 days, respectively.

The histological analyses using H&E staining discovered that DOX-cRGD30-RCCMs induced widespread tumor apoptosis but slight harm to the heart, liver, spleen and kidney (Fig. 7). Although DOX-LPs also induced massive tumor necrosis, significant damage to heart and kidney was also observed, in line with their high systemic toxicity. It should be noted that reducing dosage could lessen the toxicity of DOX-LPs but would also lead to less effective inhibition of tumor growth. All the above results point out that DOX-cRGD30-RCCMs can effectively target and treat glioma-bearing nude mice, resulting in markedly improved survival rate and reduced side effects as compared to DOX-LPs.

Our results confirm that cRGD density plays a critical role in the *in vivo* targetability and treatment efficacy for nanomedicines. Given the fact that both neovasculature and several malignant tumors over-express $\alpha_v\beta_3$ integrins [42–44,54] and that cRGD-RCCMs can load various hydrophobic drugs, cRGD-RCCMs have emerged as a extremely versatile platform for targeted tumor chemotherapy. Moreover, for different tumors, RCCMs can also be decorated with different targeting ligands [24–28]. We are currently investigating the therapeutic efficacy of DOX-cRGD-RCCMs in the orthotopic human glioma model, as several reports have shown that cRGD-functionalized nanomedicines can surpass the BBB barrier and achieve improved anti-glioma effects [44,52,56].

Please cite this article in press as: Y. Fang et al., Targeted glioma chemotherapy by cyclic RGD peptide-functionalized reversibly core-crosslinked multifunctional poly(ethylene glycol)-*b*-poly(ε-caprolactone) micelles, Acta Biomater. (2017), http://dx.doi.org/10.1016/j.actbio.2017.01.007

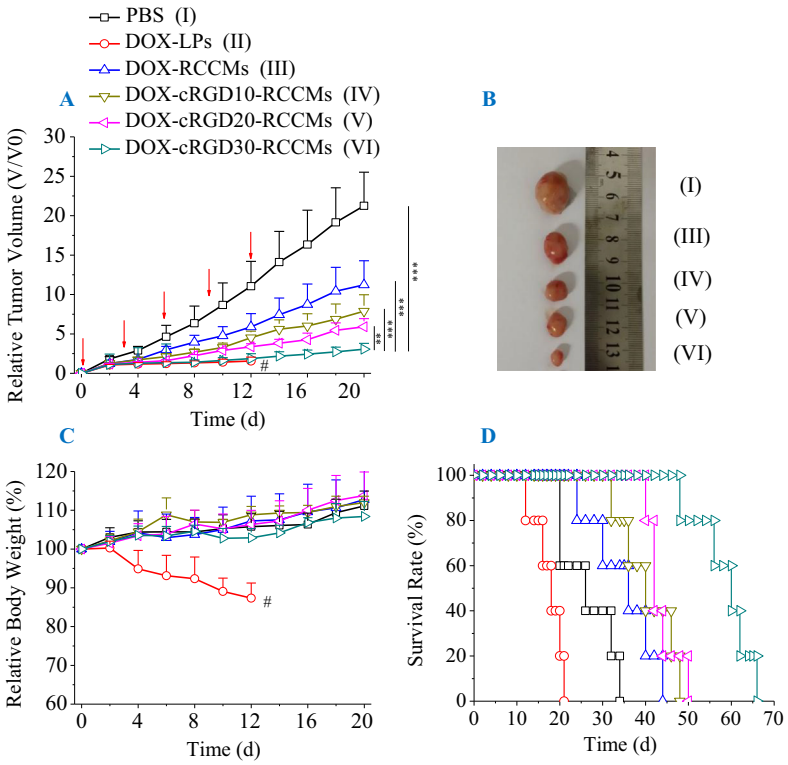

Fig. 6. The *in vivo* antitumor performance of DOX-cRGD-RCCMs and DOX-RCCMs in U87MG bearing nude mice. DOX-LPs and PBS were used as controls. The drug was given on day 0, 3, 6, 9 and 12 at 10 mg DOX/kg. (A) Tumor volume changes of mice (n = 6). Student's *t* test, $^{*}p < 0.05$, $^{**}p < 0.01$, $^{***}p < 0.001$. (B) The photographs of tumor blocks isolated on day 25. (C) The body weight changes of mice within 20 d (n = 6). (D) The survival rates of mice within 66 (n = 5). In A and C, $^{\#}$represents the point that mouse started to die.

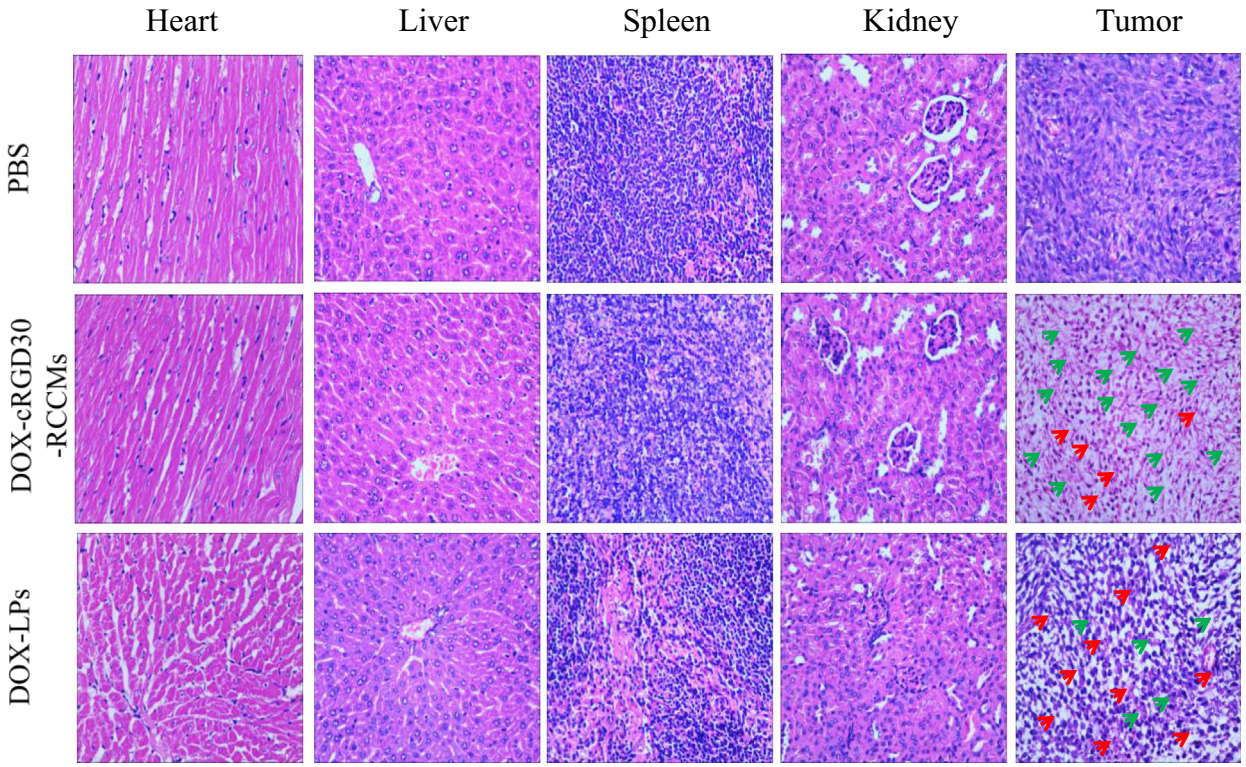

Fig. 7. Microscopic observation of H&E-stained slices of organs and tumors of U87MG tumor-bearing nude mice following 25 d treatment of DOX-cRGD30-RCCMs, DOX-LPs or PBS (40×). Green and red arrows point to tumor cell apoptosis and necrosis, respectively.

Please cite this article in press as: Y. Fang et al., Targeted glioma chemotherapy by cyclic RGD peptide-functionalized reversibly core-crosslinked multi-functional poly(ethylene glycol)-*b*-poly(ε-caprolactone) micelles, Acta Biomater. (2017), http://dx.doi.org/10.1016/j.actbio.2017.01.007

4. Conclusion

We demonstrate that cyclic RGD peptide-functionalized, rapidly glutathione-responsive, reversibly core-crosslinked micelles based on poly(ethylene glycol)-*b*-poly(ε-caprolactone) mediate highly potent and targeted glioma chemotherapy, affording significantly improved therapeutic efficacy and decreased systemic toxicity than the non-crosslinked micelles and clinically used pegylated liposomal doxorubicin. These active tumor-targeting multifunctional micellar doxorubicin has following attributes: (i) they have high drug loading capacity (~18 wt%), small size (~50 nm), high stability with low drug leakage, and fast cytoplasmic drug release; (ii) they can actively target to and be internalized by U87MG glioma cells *via* $\alpha_v\beta_3$-receptor mediated endocytosis mechanism; (iii) they show a long circulation time and efficient glioma accumulation and retention; and (iv) they are biodegradable, nontoxic, and moreover easy to prepare. These reversibly core-crosslinked biodegradable micelles based on PEG-PCL have appeared as a safe, versatile and all-function-in-one nanoplatform for targeted cancer therapy.

Acknowledgements

This work is supported by the National Natural Science Foundation of China (51273139, 51473111, 51561135010, 51225302 and 51633005), Ph.D. Programs Foundation of Ministry of Education of China (20133201110005), and the Natural Science Foundation of Jiangsu Province (14KJA150008, 14KJB150022).

Appendix A. Supplementary data

Supplementary data associated with this article can be found, in the online version, at http://dx.doi.org/10.1016/j.actbio.2017.01.007.

References

[1] V.P. Chauhan, R.K. Jain, Strategies for advancing cancer nanomedicine, Nat. Mater. 12 (2013) 958–962.
[2] A. Wicki, D. Witzigmann, V. Balasubramanian, J. Huwyler, Nanomedicine in cancer therapy: challenges, opportunities, and clinical applications, J. Controlled Release 200 (2015) 138–157.
[3] C.M. Dawidczyk, C. Kim, J.H. Park, L.M. Russell, K.H. Lee, M.G. Pomper, P.C. Searson, State-of-the-art in design rules for drug delivery platforms: lessons learned from FDA-approved nanomedicines, J. Controlled Release 187 (2014) 133–144.
[4] H. Cabral, K. Kataoka, Progress of drug-loaded polymeric micelles into clinical studies, J. Controlled Release 190 (2014) 465–476.
[5] T.Y. Kim, D.W. Kim, J.Y. Chung, S.G. Shin, S.C. Kim, D.S. Heo, N.K. Kim, Y.J. Bang, Phase I and pharmacokinetic study of Genexol-PM, a cremophor-free, polymeric micelle-formulated paclitaxel, in patients with advanced malignancies, Clin. Cancer Res. 10 (2004) 3708–3716.
[6] K. Lee, H. Chung, S. Im, Y. Park, C. Kim, S.-B. Kim, S. Rha, M. Lee, J. Ro, Multicenter phase II trial of genexol-PM, a cremophor-free, polymeric micelle formulation of paclitaxel, in patients with metastatic breast cancer, Breast Cancer Res. Treat. 108 (2008) 241–250.
[7] D.-W. Kim, S.-Y. Kim, H.-K. Kim, S.-W. Kim, S.W. Shin, J.S. Kim, K. Park, M.Y. Lee, D.S. Heo, Multicenter phase II trial of genexol-PM, a novel cremophor-free, polymeric micelle formulation of paclitaxel, with cisplatin in patients with advanced non-small-cell lung cancer, Ann. Oncol. 18 (2007) 2009–2014.
[8] J. Hrkach, D. Von Hoff, M.M. Ali, E. Andrianova, J. Auer, T. Campbell, D. De Witt, M. Figa, M. Figueiredo, A. Horhota, S. Low, K. McDonnell, E. Peeke, B. Retnarajan, A. Sabnis, E. Schnipper, J.J. Song, Y.H. Song, J. Summa, D. Tompsett, G. Troiano, T.V.G. Hoven, J. Wright, P. LoRusso, P.W. Kantoff, N.H. Bander, C. Sweeney, O.C. Farokhzad, R. Langer, S. Zale, Preclinical development and clinical translation of a PSMA-targeted docetaxel nanoparticle with a differentiated pharmacological profile, Sci. Transl. Med. 4 (2012) 128ra139.
[9] Q. Sun, M. Radosz, Y. Shen, Challenges in design of translational nanocarriers, J. Controlled Release 164 (2012) 156–169.
[10] V.P. Torchilin, Multifunctional, stimuli-sensitive nanoparticulate systems for drug delivery, Nat. Rev. Drug Discovery 13 (2014) 813–827.
[11] C. Deng, Y.J. Jiang, R. Cheng, F.H. Meng, Z.Y. Zhong, Biodegradable polymeric micelles for targeted and controlled anticancer drug delivery: Promises, progress and prospects, Nano Today 7 (2012) 467–480.
[12] Z. Ge, S. Liu, Functional block copolymer assemblies responsive to tumor and intracellular microenvironments for site-specific drug delivery and enhanced imaging performance, Chem. Soc. Rev. 42 (2013) 7289–7325.
[13] Y. Shi, R. van der Meel, B. Theek, E.O. Blenke, E.H.E. Pieters, M.H.A.M. Fens, J. Ehling, R.M. Schiffelers, G. Storm, C.F. van Nostrum, T. Lammers, W.E. Hennink, Complete regression of xenograft tumors upon targeted delivery of paclitaxel via Pi-Pi stacking stabilized polymeric micelles, ACS Nano 9 (2015) 3740–3752.
[14] S. Krishnamurthy, V.W.L. Ng, S. Gao, M.-H. Tan, Y.Y. Yang, Phenformin-loaded polymeric micelles for targeting both cancer cells and cancer stem cells in vitro and in vivo, Biomaterials 35 (2014) 9177–9186.
[15] C. Shi, H. Yu, D. Sun, L. Ma, Z. Tang, Q. Xiao, X. Chen, Cisplatin-loaded polymeric nanoparticles: characterization and potential exploitation for the treatment of non-small cell lung carcinoma, Acta Biomater. 18 (2015) 68–76.
[16] Y.-C. Wang, Y. Li, T.-M. Sun, M.-H. Xiong, J. Wu, Y.-Y. Yang, J. Wang, Core-shell-corona micelle stabilized by reversible cross-linkage for intracellular drug delivery, Macromol. Rapid Commun. 31 (2010) 1201–1206.
[17] K. Wang, G.-F. Luo, Y. Liu, C. Li, S.-X. Cheng, R.-X. Zhuo, X.-Z. Zhang, Redox-sensitive shell cross-linked PEG-polypeptide hybrid micelles for controlled drug release, Polym. Chem. 3 (2012) 1084–1090.
[18] Y.L. Li, L. Zhu, Z.Z. Liu, R. Cheng, F.H. Meng, J.H. Cui, S.J. Ji, Z.Y. Zhong, Reversibly stabilized multifunctional dextran nanoparticles efficiently deliver doxorubicin into the nuclei of cancer cells, Angew. Chem. Int. Ed. 48 (2009) 9914–9918.
[19] Y. Oe, R.J. Christie, M. Naito, S.A. Low, S. Fukushima, K. Toh, Y. Miura, Y. Matsumoto, N. Nishiyama, K. Miyata, K. Kataoka, Actively-targeted polyion complex micelles stabilized by cholesterol and disulfide cross-linking for systemic delivery of siRNA to solid tumors, Biomaterials 35 (2014) 7887–7895.
[20] Y.N. Zhong, J. Zhang, R. Cheng, C. Deng, F.H. Meng, F. Xie, Z.Y. Zhong, Reversibly crosslinked hyaluronic acid nanoparticles for active targeting and intelligent delivery of doxorubicin to drug resistant CD44+human breast tumor xenografts, J. Controlled Release 205 (2015) 144–154.
[21] X. Ke, D.J. Coady, C. Yang, A.C. Engler, J.L. Hedrick, Y.Y. Yang, PH-sensitive polycarbonate micelles for enhanced intracellular release of anticancer drugs: a strategy to circumvent multidrug resistance, Polym. Chem. 5 (2014) 2621–2628.
[22] X. Xu, W. Ho, X. Zhang, N. Bertrand, O. Farokhzad, Cancer nanomedicine: from targeted delivery to combination therapy, Trends Mol. Med. 21 (2015) 223–232.
[23] C.J. Cheng, G.T. Tietjen, J.K. Saucier-Sawyer, W.M. Saltzman, A holistic approach to targeting disease with polymeric nanoparticles, Nat. Rev. Drug Discovery 14 (2015) 239–247.
[24] S. Yang, F. Zhu, Q. Wang, F. Liang, X. Qu, Z. Gan, Z. Yang, Combinatorial targeting polymeric micelles for anti-tumor drug delivery, J. Mater. Chem. B 3 (2015) 4043–4051.
[25] H. Gao, T. Cheng, J. Liu, J. Liu, C. Yang, L. Chu, Y. Zhang, R. Ma, L. Shi, Self-regulated multifunctional collaboration of targeted nanocarriers for enhanced tumor therapy, Biomacromolecules 15 (2014) 3634–3642.
[26] J. Ahn, Y. Miura, N. Yamada, T. Chida, X. Liu, A. Kim, R. Sato, R. Tsumura, Y. Koga, M. Yasunaga, N. Nishiyama, Y. Matsumura, H. Cabral, K. Kataoka, Antibody fragment-conjugated polymeric micelles incorporating platinum drugs for targeted therapy of pancreatic cancer, Biomaterials 39 (2015) 23–30.
[27] J. Zhao, K. Babiuch, H. Lu, A. Dag, M. Gottschaldt, M.H. Stenzel, Fructose-coated nanoparticles: a promising drug nanocarrier for triple-negative breast cancer therapy, Chem. Commun. 50 (2014) 15928–15931.
[28] K. Babiuch, A. Dag, J. Zhao, H. Lu, M.H. Stenzel, Carbohydrate-specific uptake of fucosylated polymeric micelles by different cancer cell lines, Biomacromolecules 16 (2015) 1948–1957.
[29] A. Jain, A. Jain, N.K. Garg, R.K. Tyagi, B. Singh, O.P. Katare, T.J. Webster, V. Soni, Surface engineered polymeric nanocarriers mediate the delivery of transferrin-methotrexate conjugates for an improved understanding of brain cancer, Acta Biomater. 24 (2015) 140–151.
[30] K. Liang, S. Ng, F. Lee, J. Lim, J.E. Chung, S.S. Lee, M. Kurisawa, Targeted intracellular protein delivery based on hyaluronic acid-green tea catechin nanogels, Acta Biomater. 33 (2016) 142–152.
[31] R. van der Meel, L.J.C. Vehmeijer, R.J. Kok, G. Storm, E.V.B. van Gaal, Ligand-targeted particulate nanomedicines undergoing clinical evaluation: current status, Adv. Drug Delivery Rev. 65 (2013) 1284–1298.
[32] T. Lammers, F. Kiessling, W.E. Hennink, G. Storm, Drug targeting to tumors: principles, pitfalls and (pre-) clinical progress, J. Controlled Release 161 (2012) 175–187.
[33] S.C. Owen, D.P.Y. Chan, M.S. Shoichet, Polymeric micelle stability, Nano Today 7 (2012) 53–65.
[34] M. Talelli, M. Barz, C.J.F. Rijcken, F. Kiessling, W.E. Hennink, T. Lammers, Core-crosslinked polymeric micelles: principles, preparation, biomedical applications and clinical translation, Nano Today 10 (2015) 93–117.
[35] M. Barz, Complexity and simplification in the development of nanomedicines, Nanomedicine 10 (2015) 3093–3097.
[36] A.S. Hoffman, Stimuli-responsive polymers: biomedical applications and challenges for clinical translation, Adv. Drug Delivery Rev. 65 (2013) 10–16.
[37] K. Raemdonck, S.C. De Smedt, Lessons in simplicity that should shape the future of drug delivery, Nat. Biotechnol. 33 (2015) 1026–1027.
[38] Y. Min, J.M. Caster, M.J. Eblan, A.Z. Wang, Clinical translation of nanomedicine, Chem. Rev. 115 (2015) 11147–11190.

Please cite this article in press as: Y. Fang et al., Targeted glioma chemotherapy by cyclic RGD peptide-functionalized reversibly core-crosslinked multifunctional poly(ethylene glycol)-*b*-poly(ε-caprolactone) micelles, Acta Biomater. (2017), http://dx.doi.org/10.1016/j.actbio.2017.01.007

[39] A. Gabizon, M. Bradbury, U. Prabhakar, W. Zamboni, S. Libutti, P. Grodzinski, Cancer nanomedicines: closing the translational gap, Lancet 384 (2014) 2175–2176.
[40] Y. Zou, Y. Fang, H. Meng, F.H. Meng, C. Deng, J. Zhang, Z.Y. Zhong, Self-crosslinkable and intracellularly decrosslinkable biodegradable micelles: a robust, simple and multifunctional nanoplatform for high-efficiency targeted cancer chemotherapy, J. Controlled Release 244 (2016) 326–335.
[41] Y. Zou, F.H. Meng, C. Deng, Z.Y. Zhong, Robust, tumor-homing and redox-sensitive polymersomal doxorubicin: a superior alternative to doxil and caelyx?, J Controlled Release 239 (2016) 149–158.
[42] Y.N. Zhong, C. Wang, R. Cheng, L. Cheng, F.H. Meng, Z. Liu, Z.Y. Zhong, CRGD-directed, NIR-responsive and robust AuNR/PEG-PCL hybrid nanoparticles for targeted chemotherapy of glioblastoma in vivo, J. Controlled Release 195 (2014) 63–71.
[43] N. Nasongkla, X. Shuai, H. Ai, B.D. Weinberg, J. Pink, D.A. Boothman, J.M. Gao, CRGD-functionalized polymer micelles for targeted doxorubicin delivery, Angew. Chem. Int. Ed. 43 (2004) 6323–6327.
[44] Y. Miura, T. Takenaka, K. Toh, S. Wu, H. Nishihara, M.R. Kano, Y. Ino, T. Nomoto, Y. Matsumoto, H. Koyama, H. Cabral, N. Nishiyama, K. Kataoka, Cyclic RGD-linked polymeric micelles for targeted delivery of platinum anticancer drugs to glioblastoma through the blood-brain tumor barrier, ACS Nano 7 (2013) 8583–8592.
[45] Y.Q. Zhu, J. Zhang, F.H. Meng, C. Deng, R. Cheng, F.J. Jan, Z.Y. Zhong, CRGD-functionalized reduction-sensitive shell-sheddable biodegradable micelles mediate enhanced doxorubicin delivery to human glioma xenografts in vivo, J. Controlled Release 233 (2016) 29–38.
[46] C. Dingels, F. Wurm, M. Wagner, H.A. Klok, H. Frey, Squaric acid mediated chemoselective PEGylation of proteins: reactivity of single-step-activated alpha-amino poly(ethylene glycol)s, Chemistry 18 (2012) 16828–16835.
[47] F. Wurm, C. Dingels, H. Frey, H.A. Klok, Squaric acid mediated synthesis and biological activity of a library of linear and hyperbranched poly(glycerol)-protein conjugates, Biomacromolecules 13 (2012) 1161–1171.
[48] C. Schieber, A. Bestetti, J.P. Lim, A.D. Ryan, T.-L. Nguyen, R. Eldridge, A.R. White, P.A. Gleeson, P.S. Donnelly, S.J. Williams, P. Mulvaney, Conjugation of transferrin to azide-modified CdSe/ZnS core-shell quantum dots using cyclooctyne click chemistry, Angew. Chem. Int. Ed. 51 (2012) 10523–10527.
[49] D. Sutton, S. Wang, N. Nasongkla, J.M. Gao, E.E. Dormidontova, Doxorubicin and beta-lapachone release and interaction with micellar core materials: experiment and modeling, Exp. Biol. Med. 232 (2007) 1090–1099.
[50] J. Yan, Z. Ye, M. Chen, Z. Liu, Y. Xiao, Y. Zhang, Y. Zhou, W. Tan, M. Lang, Fine tuning micellar core-forming block of poly(ethylene glycol)-block-poly (epsilon-caprolactone) amphiphilic copolymers based on chemical modification for the solubilization and delivery of doxorubicin, Biomacromolecules 12 (2011) 2562–2572.
[51] P. Mohan, N. Rapoport, Doxorubicin as a molecular nanotheranostic agent: effect of doxorubicin encapsulation in micelles or nanoemulsions on the ultrasound-mediated intracellular delivery and nuclear trafficking, Mol. Pharm. 7 (2010) 1959–1973.
[52] J. Choi, J. Yang, J. Park, E. Kim, J.-S. Suh, Y.-M. Huh, S. Haam, Specific near-IR absorption imaging of glioblastomas using integrin-targeting gold nanorods, Adv. Funct. Mater. 21 (2011) 1082–1088.
[53] C.J. Rijcken, C.J. Snel, R.M. Schiffelers, C.F. van Nostrum, W.E. Hennink, Hydrolysable core-crosslinked thermosensitive polymeric micelles: synthesis, characterisation and in vivo studies, Biomaterials 28 (2007) 5581–5593.
[54] Y. Xiao, H. Hong, A. Javadi, J.W. Engle, W. Xu, Y. Yang, Y. Zhang, T.E. Barnhart, W. Cai, S. Gong, Multifunctional unimolecular micelles for cancer-targeted drug delivery and positron emission tomography imaging, Biomaterials 33 (2012) 3071–3082.
[55] H.-W. Kao, C.-J. Chan, Y.-C. Chang, Y.-H. Hsu, M. Lu, J.S.-J. Wang, Y.-Y. Lin, S.-J. Wang, H.-E. Wang, A pharmacokinetics study of radiolabeled micelles of a poly (ethylene glycol)-block-poly(caprolactone) copolymer in a colon carcinoma-bearing mouse model, Appl. Radiat. Isot. 80 (2013) 88–94.
[56] W. Kawamura, Y. Miura, D. Kokuryo, K. Toh, N. Yamada, T. Nomoto, Y. Matsumoto, D. Sueyoshi, X. Liu, I. Aoki, M.R. Kano, N. Nishiyama, T. Saga, A. Kishimura, K. Kataoka, Density-tunable conjugation of cyclic RGD ligands with polyion complex vesicles for the neovascular imaging of orthotopic glioblastomas, Sci. Technol. Adv. Mater. 16 (2015) 035004.

Please cite this article in press as: Y. Fang et al., Targeted glioma chemotherapy by cyclic RGD peptide-functionalized reversibly core-crosslinked multi-functional poly(ethylene glycol)-*b*-poly(ε-caprolactone) micelles, Acta Biomater. (2017), http://dx.doi.org/10.1016/j.actbio.2017.01.007